IMPLEMENTING MULTI-SCALE AGRICULTURAL INDICATORS EXPLOITING SENTINELS

VEGETATION FIELD DATA AND PRODUCTION OF GROUND-BASED MAPS:

"LAS TIESAS - BARRAX SITE, ALBACETE, SPAIN" 29TH- 30TH MAY 2014

ISSUE I1.10

EC Proposal Reference N° FP7-311766

Actual submission date : September 2015

Start date of project: 01.11.2012   Duration : 40 months

Name of lead partner for this deliverable: EOLAB

Book Captain: Consuelo Latorre (EOLAB)

Contributing Authors: Fernando Camacho (EOLAB)

F. de la Cruz, F. Atienzar (ITAP)

Project co-funded by the European Commission within the Seventh Framework Program (2007-2013)		
Dissemination Level		
PU	Public	**X**
PP	Restricted to other programme participants (including the Commission Services)	
RE	Restricted to a group specified by the consortium (including the Commission Services)	
CO	Confidential, only for members of the consortium (including the Commission Services)	

DOCUMENT RELEASE SHEET

Book Captain:	C. Latorre	Date: 03.09.2015	Sign.
Approval:	R. Lacaze	Date: 24.09.2015	Sign.
Endorsement:	I. Marin-Moreno	Date:	Sign.
Distribution:	Public		

CHANGE RECORD

Issue/Revision	Date	Page(s)	Description of Change	Release
	08.05.2015	All	First Issue	I1.00
	03.09.2015	24 - 38	Maps based on TOC reflectances and NDVI combination	I1.10

TABLE OF CONTENTS

LIST OF FIGURES

LIST OF TABLES

LIST OF ACRONYMS

CEOS	Committee on Earth Observation Satellite
CEOS LPV	Land Product Validation Subgroup
DG AGRI	Directorate General for Agriculture and Rural Development
DG RELEX	Directorate General for External Relations (European Commission)
DHP	Digital Hemispheric Photographs
ECV	Essential Climate Variables
EUROSTATS	Directorate General of the European Commission
ESU	Elementary Sampling Unit
FAPAR	Fraction of Absorbed Photo-synthetically Active Radiation
FAO	Food and Agriculture Organization
FCOVER	Fraction of Vegetation Cover
GCOS	Global Climate Observing System
GEO-GLAM	Global Agricultural Geo- Monitoring Initiative
GIO-GL	GMES Initial Operations - Global Land (GMES)
GCOS	Global Climate Observing System
GMES	Global Monitoring for Environment and Security
GPS	Global Positioning System
IMAGINES	Implementing Multi-scale Agricultural Indicators Exploiting Sentinels
ITAP	*Instituto Técnico Agronómico Provincial – Diputación de Albacete*.
JECAM	Joint Experiment for Crop Assessment and Monitoring
LAI	Leaf Area Index
LDAS	Land Data Assimilation System
LUT	Look-up-table techniques
PAI	Plant Area Index
PASTIS –PAR	PAI Autonomous System from Transmittance Sensors.
PROBA-V	Project for On-Board Autonomy satellite, the V standing for vegetation.
RMSE	Root Mean Square Error
SPOT /VGT	Satellite Pour l'Observation de la Terre / VEGETATION
SCI	GMES Services Coordinated Interface
SLT	Solar Local Time
TOC	Top of Canopy Reflectance
USGS	U.S. Geological Survey Science organization.
UNFCCC	United Nations Framework Convention on Climate Change
UTM	Universal Transverse Mercator coordinates system
VALERI	Validation of Land European Remote sensing Instruments
WGCV	Working Group on Calibration and Validation (CEOS)

1. BACKGROUND OF THE DOCUMENT

1.1. EXECUTIVE SUMMARY

The Copernicus Land Service has been built in the framework of the FP7 geoland2 project, which has set up pre-operational infrastructures. ImagineS intends to ensure the continuity of the innovation and development activities of geoland2 to support the operations of the global land component of the GMES Initial Operation (GIO) phase. In particular, the use of the future Sentinel data in an operational context will be prepared. Moreover, IMAGINES will favor the emergence of new downstream activities dedicated to the monitoring of crop and fodder production.

The main objectives of ImagineS are to (i) improve the retrieval of basic biophysical variables, mainly LAI, FAPAR and the surface albedo, identified as Terrestrial Essential Climate Variables, by merging the information coming from different sensors (PROBA-V and Landsat-8) in view to prepare the use of Sentinel missions data; (ii) develop qualified software able to process multi-sensor data at the global scale on a fully automatic basis; (iii) complement and contribute to the existing or future agricultural services by providing new data streams relying upon an original method to assess the above-ground biomass, based on the assimilation of satellite products in a Land Data Assimilation System (LDAS) in order to monitor the crop/fodder biomass production together with the carbon and water fluxes;(iv) demonstrate the added value of this contribution for a community of users acting at global, European, national, and regional scales.

Further, ImagineS will serve the growing needs of international (e.g. FAO and NGOs), European (e.g. DG AGRI, EUROSTATS, DG RELEX), and national users (e.g. national services in agro-meteorology, ministries, group of producers, traders) on accurate and reliable information for the implementation of the EU Common Agricultural Policy, of the food security policy, for early warning systems, and trading issues. ImagineS will also contribute to the Global Agricultural Geo-Monitoring Initiative (GEO-GLAM) by its original agriculture service which can monitor crop and fodder production together with the carbon and water fluxes and can provide drought indicators, and through links with JECAM (Joint Experiment for Crop Assessment and Monitoring).

1.2. PORTFOLIO

The ImagineS portfolio contains global and regional biophysical variables derived from multi-sensor satellite data, at different spatial resolutions, together with agricultural indicators, including the above-ground biomass, the carbon and water fluxes, and drought indices resulting from the assimilation of the biophysical variables in the Land Data Assimilation System (LDAS).

The production in Near Real Time of the 333m resolution products, at a frequency of 10 days, using PROBA-V data will be carried out in the Copernicus Global Land Service. It should start by covering Europe only, and be gradually extended to the whole globe.

Meanwhile, ImagineS will perform in parallel off-line production over demonstration sites outside Europe. The demonstration of high resolution (30m) products (Landsat-8 + PROBA-

V) will be done over demonstration sites of cropland and grassland in contrasting climatic and environmental conditions.

1.3. SCOPE AND OBJECTIVES

The main objective of this document is to describe the field campaign and ground data collected at Las Tiesas site in Barrax, Spain, and the up-scaling of the ground data to produce ground-based high resolution maps of the following biophysical variables:

- Leaf Area Index (LAI), defined as half of the total developed area of leaves per unit ground surface area (m^2/m^2). We focused on two different LAI quantities (for green elements):
  - ➢ The effective LAI (LAIeff) derived from the description of the gap fraction as a function of the view zenith angle. In addition, effective LAI measures derived at 57.5º are also provided in the ground database.
  - ➢ The actual LAI (LAI) estimate corrected from the clumping index.
- Fraction of green vegetation cover (FCover), defined as the proportion of soil covered by vegetation, derived from the gap fraction between 0 and 10º of view zenith angle.
- Fraction of Absorbed Photosynthetically Active Radiation (FAPAR), which is the fraction of the photosynthetically active radiation (PAR) absorbed by a vegetation canopy. We are also focused on green elements. PAR is the solar radiation reaching the canopy in the 0.4–0.7 µm wavelength region. We focused on the instantaneous 'black-sky' FAPAR at 10:00h Solar Local Time (SLT), which is the FAPAR under direct illumination conditions at a given solar position. In addition, two other quantities are provided: daily integrated FAPAR computed as the black-sky FAPAR integrated over the day and the 'white-sky' FAPAR, which is the FAPAR under diffuse illumination conditions.

1.4. CONTENT OF THE DOCUMENT

This document is structured as follows:

- Chapter 2 provides an introduction to the field experiment.
- Chapter 3 provides the location and description of the site.
- Chapter 4 describes the ground measurements, including material and methods, sampling and data processing.
- Chapter 5 provides an evaluation of the sampling.
- Chapter 6 describes the production of high resolution ground-based maps, and the selected "mean" values for validation.

2. INTRODUCTION

Validation of remote sensing products is mandatory to guaranty that the satellite products meets the user's requirements. Protocols for validation of global LAIeff products are already developed in the context of Land Product Validation (LPV) group of the Committee on Earth Observation Satellite (CEOS) for the validation of satellite-derived land products (Fernandes et al., 2014), and recently applied to Copernicus global land products based on SPOT/VGT observation (Camacho et al., 2013). This generic approach is made of 2 major components:

- The indirect validation: including inter-comparison between products as well as evaluation of their temporal and spatial consistency
- The direct validation: comparing satellite products to ground measurements of the corresponding biophysical variables. In the case of low and medium resolution sensors, the main difficulty relies on scaling local ground measurements to the extent corresponding to pixels size. However, the direct validation is limited by the small number of sites, for that reason a main objective of ImagineS is the collection of ground truth data in demonstration sites.

The content of this document is compliant with existing validation guidelines (for direct validation) as proposed by the CEOS LPV group (Morisette et al., 2006); the VALERI project (http://w3.avignon.inra.fr/valeri/) and ESA campaigns (Baret and Fernandes, 2012). It therefore follows the general strategy based on a bottom up approach: it starts from the scale of the individual measurements that are aggregated over an elementary sampling unit (ESU) corresponding to a support area consistent with that of the high resolution imagery used for the up-scaling of ground data. Several ESUs are sampled over the site. Radiometric values over a decametric image are also extracted over the ESUs. This will be later used to develop empirical transfer functions for up-scaling the ESU ground measurements (e.g. Martínez et al., 2009). Finally, the high resolution ground based map will be compared with the medium resolution satellite product at the spatial support of the product.

One of the demonstration sites of ImagineS is located in the experimental farm of Las Tiesas in Barrax (Albacete, Spain), where a large number of ESA cal/val campaigns were conducted (e.g. Berguer et al., 2001) due to its favorable conditions. Furthermore, this area is a pilot area for downstream applications on irrigation and farming advisory systems from earth observation data (Calera et al., 2005).

In the framework of ImagineS a field experiment was conducted in collaboration with ITAP (*Instituto Técnico Agronómico Provincial)* for the spatial and temporal characterization of the vegetation properties. Two main activities were conducted: (1) an intensive field campaign on 29th - 30th May, 2014 with Digital Hemispherical Photos (DHP) for the spatial characterization of vegetation variables in the study area, conducted by EOLAB, and (2) set-up of PASTIS-PAR (PAI Autonomous System from Transmittance Sensors) systems for the continuous monitoring of FAPAR and Plant Area Index (PAI) during the spring and summer time, conducted by the ITAP under a subcontract with EOLAB (Ref No FP7-311766-14/1).

The PASTIS-PAR sensors developed by INRA were installed for spring and summer crops from April to August.

This report describes the ground activities during the intensive field campaign. The results of the PASTIS-PAR data recorded are under analysis by INRA-Avignon and the main results will be reported separately.

Intensive Field Campaign: 29th - 30th of May 2014.

Contact:

EOLAB: Fernando Camacho (fernando.camacho@eolab.es)

ITAP: F. De la Cruz (fct.itap@dipualba.es)

Teams involved in field collection (Figure 1**):**

ITAP: F. De la Cruz, F. Atienzar

EOLAB: F. Camacho, C. Latorre

Figure 1: People involved in the field campaign of Las Tiesas site in Barrax, Spain. The images were taken in a field of corn where the PASTIS-PAR devices were installed.

3. STUDY AREA

3.1. LOCATION

The experimental site is located around 'Las Tiesas' farm in Barrax. Barrax belongs to the province of Albacete, 200 km away from Valencia and 20 km away from Albacete town (see Figure 2).
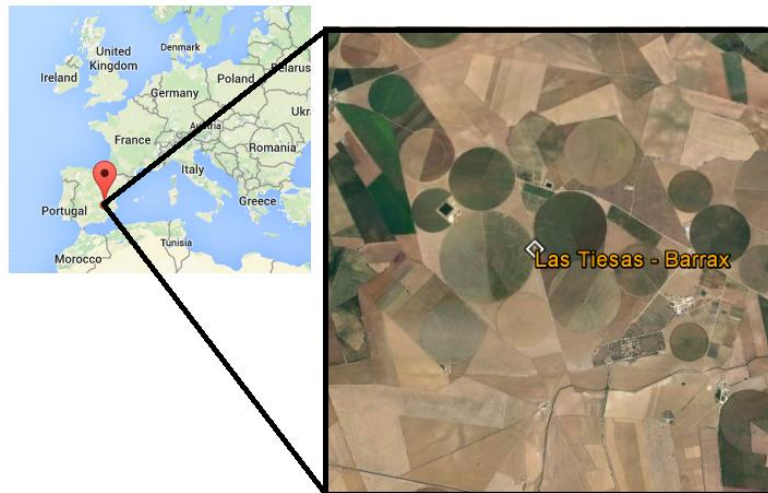
Figure 2: Location of Las Tiesas site in Barrax, Spain.

Table 1: Coordinates and altitude of the test site (centre).

Site Center	
Geographic Lat/lon, WGS-84 (degrees)	Latitude = 39.054371 N Longitude = 2.100677 W
Altitude	700 m

Figure 3 shows the false composition Red Green Blue (RGB) over a Top Of Canopy (TOC) Reflectance Landsat-8 image.
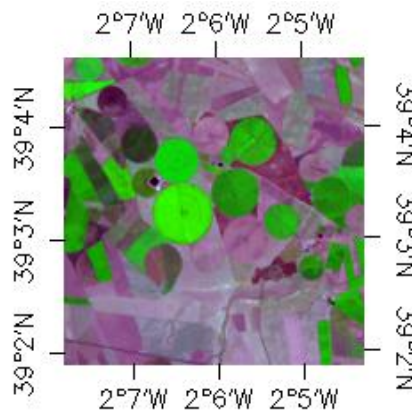
Figure 3: False color composition (RGB – SWIR-NIR-RED) of TOC Reflectance Landsat-8 image over the study area 5 km x 5 km. (Barrax, 26th May 2014).

3.2 DESCRIPTION OF THE TEST SITE

Barrax test site is situated within La Mancha, a plateau 700 m above sea level. The test site is located in the west of province of Albacete. It is 20 km far away from the capital town Albacete. The area is characterized by a flat morphology with large and uniform land units. Differences in elevation range up to 2 m only. The regional water table is about 20-30 m below the land surface.

The climatic conditions accord the Mediterranean features: high precipitations in spring and autumn and the minimum in summer. The annual rainfall averages is about 400 mm. Furthermore, the region has high continentally with high thermal oscillations during all seasons. La Mancha represents one of the driest regions of Europe. The region consists of approximately 65% dry land and 35% irrigated land with different agricultural fields.

Figure 4 shows the land use map during the field campaign. Camelina (Ca) and Barley (B) fields were senescent at the time of the field campaign, and many other fields were harvested. Among the irrigated fields we found Corn (C) crops at different stage of development, Onion (O), Wheat (W), Garlic (G), Potato (P) and Sunflower (S) among other crop types in minor proportion (e.g., vineyard, fruit trees, papaver somniferum (poppy)). These crop types are well representative of the crops of the region.
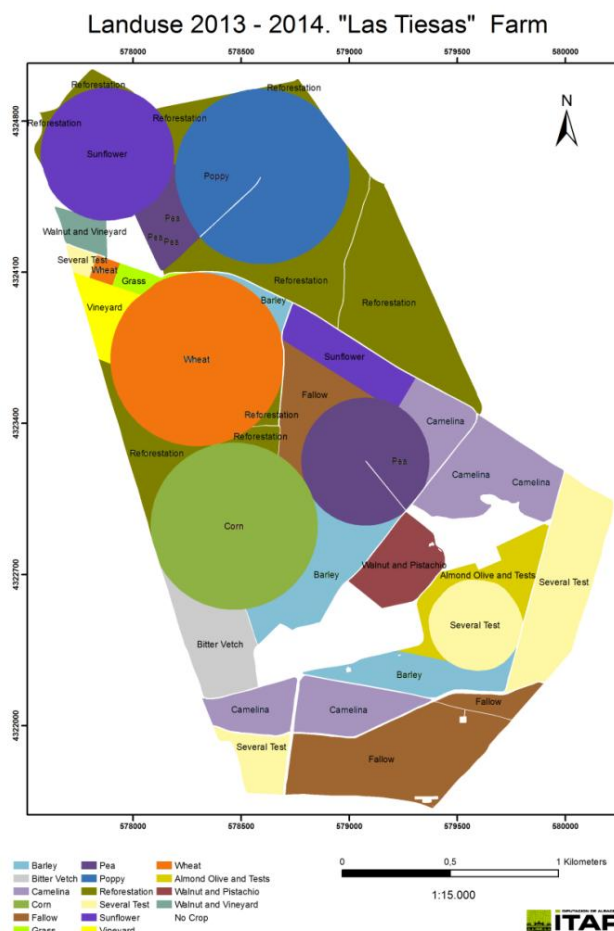
Figure 4: Land use map of Las Tiesas, Barrax (Spain).

4. GROUND MEASUREMENTS

The ground measurement database reported here was acquired by EOLAB.

4.1. MATERIAL AND METHODS

Several devices were used for estimating biophysical variables in the study area, including hemispherical digital photography (DHP).

Digital Hemispheric Photographs (DHP) were acquired with a digital camera. Hemispherical photos allow the calculation of LAI, FAPAR and FCOVER measuring gap fraction through an extreme wide-angle camera lens (i.e. 180º) (Weiss et al., 2004). It produces circular images that record the size, shape, and location of gaps, either looking upward from within a canopy or looking downward from above the canopy. The system is composed by a professional camera and a fisheye lens: CANON EOS 6D and a SIGMA 8mm F3.5 – EX DG.

Since optical systems are not perfect, it is needed to calibrate the system in order to determinate the Optical Centre and the Projection Function (Weiss, 2010). The optical centre is defined by the projection of the optical axis onto the CCD matrix where the image is recorded, for our dual system (camera and lens) was found in the point: (x=1378, y=896) (Latorre et al. 2014).

The hemispherical photos acquired during the field campaign were processed with the CAN-EYE software version 6.3.12 (developed by INRA http://www6.paca.inra.fr/can-eye) to derive LAI, FAPAR and FCOVER. It is based on a RGB colour classification of the image to discriminate vegetation elements from background (i.e., gaps). This approach allows exploiting downward-looking photographs for short canopies (background = soil) as well as upward-looking photographs for tall canopies (background = sky). CAN-EYE software processes simultaneously up to of 20 images acquired over the same ESU. Note that our images were acquired with similar illumination conditions to limit the variation of colour dynamics between images.

The processing is achieved in 3 main steps (Weiss et al., 2004). First, image pre-processing is performed, which includes removing undesired objects (e.g. operator, sun glint) and image contrast adjustments to ensure a better visual discrimination between vegetation elements and background. Second, an automatic classification (k-means clustering) is applied to reduce the total number of distinctive colours of the image to 324 which is sufficient to ensure accurate discrimination capacities while keeping a small enough number of colours to be easily manipulated. Finally, a default classification based on predefined colour segmentation is first proposed and then iteratively refined by the user. The allocation of the colours to each class (vegetation elements versus background) is the most critical phase that needs to be interactive because colours depend both on illumination conditions and on canopy elements. At the end of this process a binary image, background versus vegetation elements (including both green and non-green elements) is obtained.

The CAN-EYE software computes biophysical variables from gap fraction as follows:

Effective LAI (LAIeff): Among the several methods described in Weiss et al (2004), the effective LAI estimation in the CAN-EYE software is performed by model inversion. The effective LAI is estimated from the Plant Area Index (PAI) which is the variable estimated by CAN-EYE, as no distinction between leaves or other plant elements are made from the gap fraction estimates. PAI is very close to the effective LAI for croplands when pictures are taken downward looking, whereas larger discrepancies are expected for forest when pictures are taken upward looking. Effective LAI is directly retrieved by inverting Eq. (1) (Poisson model) and assuming an ellipsoidal distribution of the leaf inclination using look-up-table (LUT) techniques.

$$P_0(\theta_v, \varphi_v) = e^{-N \cdot (\theta_v, \varphi_v)} = e^{-G \cdot (\theta_v, \varphi_v) \cdot \frac{LAI_{eff}}{\cos(\theta_v)}}$$

Eq. (1)

A large range of random combinations of LAI (between 0 and 10, step of 0.01) and ALA (Average Leaf Angle)(10º and 80º, step of 2º) values is used to build a database made of the corresponding gap fraction values (Eq.1) in the zenithal directions defined by the CAN-EYE user (60º for the DHP collection in this field campaign). The process consists then in selecting the LUT element in the database that is the closest to the measured P_0. The distance (cost function C_k) of the kth element of the LUT to the measured gap fraction is computed as the sum of two terms. The first term computes a weighted relative root mean square error between the measured gap fraction and the LUT one. The second term is the regularization term that imposes constraints to improve the PAI estimates. Two equations are proposed for the second "regularization" term:

(1) constraint used in CAN-EYE V5.1 on the retrieved ALA values that assume an average leaf angle close to 60º ± 03º, and

(2) constraint used in CAN-EYE V6.1 on the retrieved PAI value that must be close from the one retrieved from the zenithal ring at 57º. This constraint is more efficient, but it can be computed only when the 57º ring is available (i.e., COI≥60º)

The software also proposed other ways of computing PAI and ALA effective using Miller's formula (Miller, 1967) which assumed that gap fraction only depends from view zenith angle. Furthermore, the CAN-EYE makes an estimation using the Welles and Norman (1991) method used in LAI-2000 for 5 rings. These LAI2000-like estimates were not used here as are based on the same Miller's formula but using limited angular sampling.

LAI: The actual LAI that can be measured only with a planimeter with however possible allometric relationships to reduce the sampling, is related to the effective leaf area index through:

$$LAI_{eff} = \lambda_0 \cdot LAI$$

Eq. (2)

where λ_0 is the clumping index. In CAN-EYE, the clumping index is computed using the Lang and Xiang (1986) logarithm gap fraction averaging method, although some uncertainties are associated to this method (Demarez et al., 2008). The principle is based on the assumption that vegetation elements are locally assumed randomly distributed. Values of clumping index given by CAN_EYE are in certain cases correlated with the size of the cells used to divide photographs. The values reported here were estimated with an average of the three results (CEV6.1, CEV5.1 and Miller).

*As the CAN-EYE software provides different results (CEV6.1, CEV5.1 and Miller's) for LAI and LAIeff variables; an average LAI value was provided as ground estimate, and the standard deviation of the different method LAI estimates was reported as the uncertainty of the estimate (see associated **20140529_VGM_LasTiesas_Barrax.xls** file)*

FCOVER is retrieved from gap fraction between 0 to 10°.

$$FCOVER = 1 - P_0 \cdot (0 - 10°)$$
Eq. (3)

FAPAR: As there is little scattering by leaves in that particular spectral domain due to the strong absorbing features of the photosynthetic pigments, FAPAR is often assumed to be equal to FIPAR (Fraction of Intercepted Photosynthetically Active Radiation), and therefore directly related to the gap fraction. The actual FAPAR is the sum of two terms, weighted by the diffuse fraction in the PAR domain: the 'black sky' FAPAR that corresponds to the direct component and the 'white sky' or the diffuse component.

The instantaneous "Black-sky FAPAR" (FPAR[BS]) is given at a solar position (date, hour and latitude). Depending on latitude, the CAN EYE software computes the solar zenith angle every solar hour during half the day (there is symmetry at 12:00). The instantaneous FAPAR is then approximated at each solar hour as 1 minus the gap fraction in the corresponding solar zenith angle:

$$FAPAR^{BS}(\theta_S) = 1 - P_0 \cdot (\theta_S)$$
Eq. (4)

The daily integrated black sky or direct FAPAR is computed as the following:

$$FAPAR_{Day}^{BS} = \frac{\int_{sunset}^{sunrise} cos(\theta_S) \cdot [1 - P_0 \cdot (\theta_S)] \cdot d\theta}{\int_{sunset}^{sunrise} cos(\theta_S) \cdot d\theta}$$
Eq. (5)

The CAN-EYE software provides FAPAR Instantaneous and FAPAR daily integrated values as well. FAPAR instantaneous at 10:00 a.m. SLT was up-scaled.

4.2. SPATIAL SAMPLING SCHEME

A pseudo-regular sampling was used within each Elementary Sampling Unit (ESU) of approximately 20x20 m^2. The centre of the ESU was geo-located using a Global Positioning System (GPS). A total of 30 ESUs of 11 different land cover types were characterized during the campaign (see Figure 5). The number of hemispherical photos per ESU ranges between 12 and 15. In several ESUs, continuous measurements were taken with PASTIS-PAR devices for monitoring the seasonal cycle (*Table 2*).
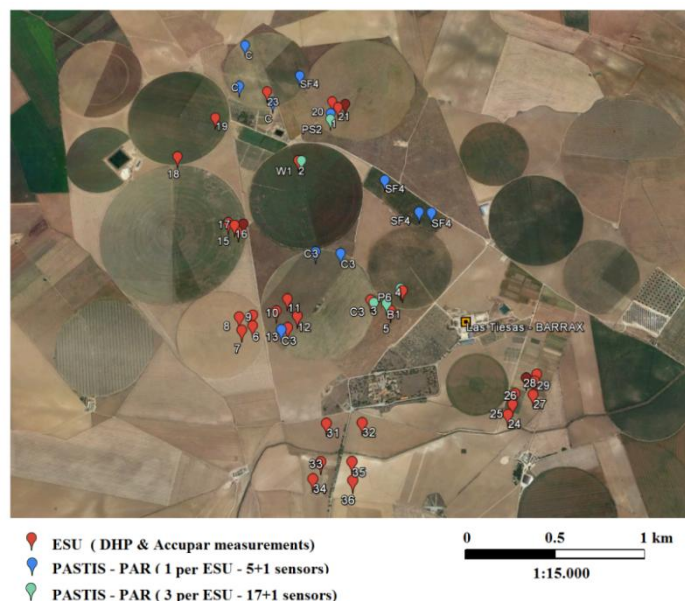
Figure 5: Distribution of the sampling units (ESU) over the study area. DHP sampling (red), over Las Tiesas site, Barrax - Albacete (Spain). Blue and Green for PASTIS-PAR sampling.

Table 2: Location of PASTIS-PAR systems, ID, coordinates, period, area, and average value measured the day of the intensive field campaign.

ESU	PASTIS	COORDINATES		PERIOD		FAPAR 29th May, 2014	AREA (ha)
		Latitude	Longitude	Initial	End		
WHEAT - Pivot 1	500	39.059	-2.097	01/04/2014	30/06/2014	0.851	50.70 ha
	503						
	511						
BARLEY	495	39.050	-2.089	01/04/2014	03/06/2014	0.119	14.26 ha
	506						
	507						
PEA - Pivot 6	493	39.051	-2.088	16/04/2014	09/06/2014	1.000	27.51 ha
	497						
	509						
PAPPAVER - Pivot 2	502	39.062	-2.095	23/04/2014	14/07/2014	1.000	50.44 ha
	525						
	528						
CORN - Pivot 3	521	39.050	-2.090	19/05/2014	11/08/2014	0.258	46.98 ha
	523						
	526						
	506	39.053	-2.095	06/06/2014	11/08/2014	0.295	
	507	39.053	-2.093			0.271	
	480	39.048	-2.097			0.233	
SUNFLOWER - Pivot 4	509	39.056	-2.086	10/06/2014	29/08/2014	0.389	29.88 ha
	495	39.056	-2.087			0.346	
	493	39.058	-2.090			0.377	
CORN	497	39.065	-2.098	13/06/2014	29/08/2014	0.292	11.18 ha
	515	39.063	-2.100			0.273	
	548	39.064	-2.103			0.253	
	542	39.067	-2.103			0.129	

The spatial sampling scheme was predefined to cover the existing variability over the study area. Additional elementary sampling units (ESU) were selected to complete the representation of the vegetation cover types presented in the study area, such as Bare Soil (BS) and senescent crops (i.e. Wheat, Barley and Camelina) where vegetation measurements were estimated by visual inspection either because it corresponds to bare areas or to completely dry (i.e, Non-Photosynthetically active Vegetation, NPV). The proportion of both bare areas and NPV crops were quite large in the study area during the field campaign. The distribution of the ESUs in the study area is shown in figure 6.

Figure 6 summarizes the number of sampling units per each crop type acquired during the field campaign (30 ESUS).The percentage of the several vegetation types sampled was 21% of corn in early stage of growing and 12% of sampling was wheat fields. The other more representative crops were: papaver, onion and alfalfa crops.

Distribution of 30 ESUS over BARRAX site

Intensive Field campaign 29th - 30th

PS (Papaver Somniferum)
W (Wheat)
C (Corn)
P (Pea)
ON (Onion)
AL (Alfalfa)
R (Rape)
P (Potato)
SF(Sunflower)
Ca (Camelina)
B (Barley)
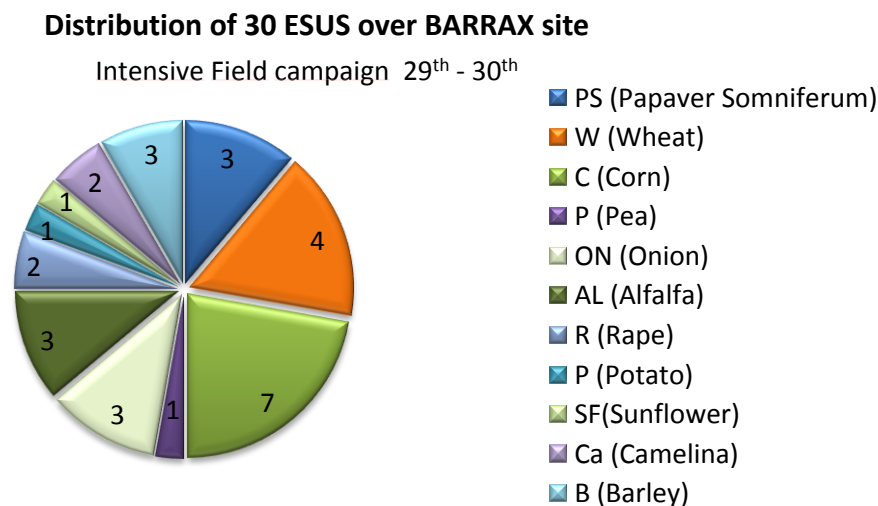
Figure 6: Distribution of vegetation types sampled during the intensive campaign. *Las Tiesas site – Barrax (Spain).*

4.3. GROUND DATA

4.3.1. Data processing

The software CAN-EYE version V 6.3.12 was used to process the DHP images. Figure 7 shows some examples of DHP over several ESUs. Note the low vegetated coverage of the corn fields.
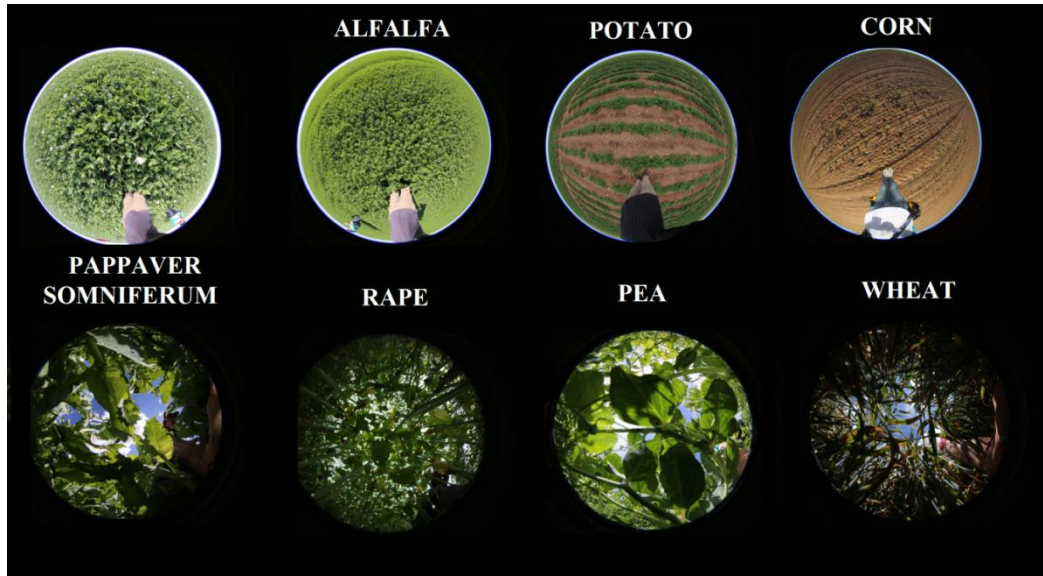
Figure 7: Digital Hemispherical Photographs acquired in Las Tiesas site, Barrax (Spain) during the intensive campaign of 29 - 30 May 2014.

Figure 8 shows the results of the CAN-EYE processing carried out on a cultivated area (Corn – ESU 20). Different results of the CAN-EYE processing are selected: the masking, the classification of vegetation and the image generated by the software. Other graphs are shown: the average gap fraction and the clumpling factor versus view zenith angle.

Figure 8: Results of the CAN-EYE processing carried out on cultivate area (ESU 20, Corn). (a) DHP images. (b, c) Classified images. (d) Average gap fraction and (e) the clumping factor versus view zenith angle.

As described at section 4.1, the LAI and effective LAI values were calculated with the average of different estimations (CEV6.1, CEV5.1 and Miller's). Figure 9 shows the inter-comparison between the three methods. For LAIeff, the results are very similar, however for the LAI graph, the variation between methods is higher for medium values. Miller's method presents the lowest estimations.
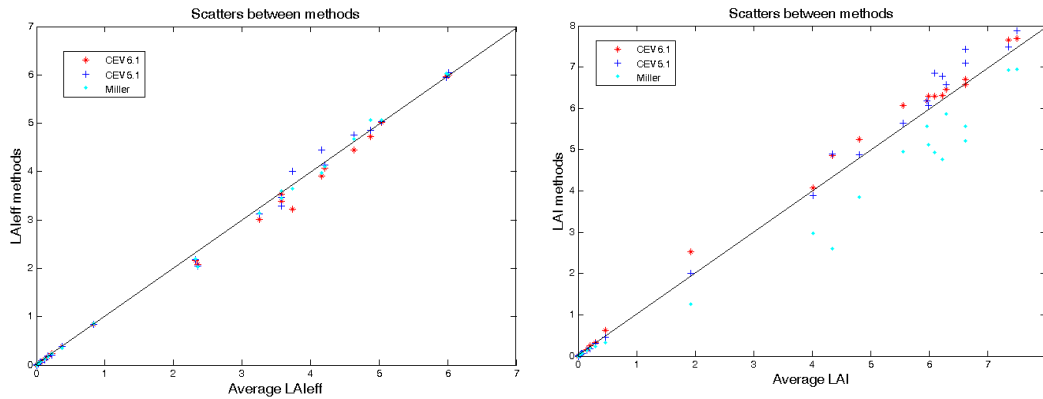
Figure 9: Inter-comparison of the calculated biophysical variables LAI and LAIeff over the ESUs with different methods: CEV5.1, CEV6.1 and Miller´s formula. Las Tiesas site – Barrax (Spain) during the campaign of 29th May, 2014.

Figure 10 shows the intercomparison between LAI and effective LAI with instantaneous FAPAR at 10 a.m. SLT. The typical positive exponential curve is observed, most clearly for LAIeff, LAI Miller's method presents more differences with CAN-EYE estimates for high values.
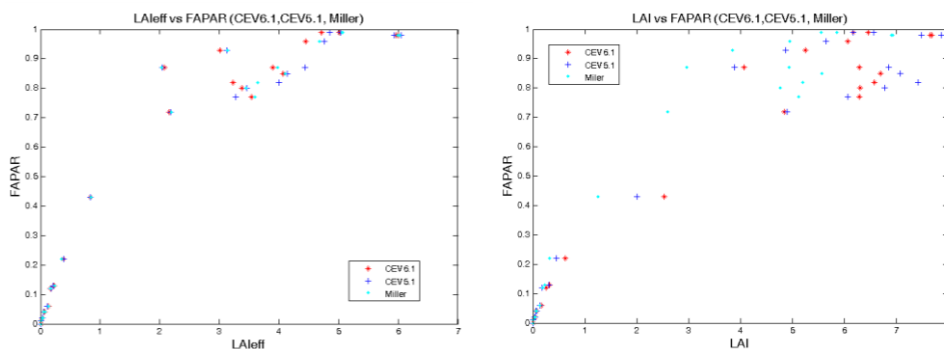
Figure 10: Intercomparison of the measured biophysical variables over the ESUs. Effective LAI and LAI versus FAPAR, Las Tiesas site – Barrax (Spain) during the campaign of 29th May, 2014.

4.3.1.1. *Special cases*

For the very homogeneous alfalfa and papaver cover, the acquisition should be taken from above (downward looking) in order to not modify the state of the vegetation canopy. Figure 11 shows the example of the photo taken downward looking and upward looking. As it can be observed, the camera disturbs the natural state of the plant canopy and opens a large gap fraction around the zenith, which will introduce an important underestimation in the vegetation parameters. We have processed the downward looking pictures which provide very high vegetation values as no soil elements are observed.

Figure 11: ESU (12) alfalfa and ESU (21) Papaver somniferum fields.

Figure 12 shows several DHP images for the ESU-6 located on an Onion field where the crop are contaminated with grass providing quite heterogeneous samples. The data processing is thus quite influenced by the spatial variability of the DHP collection over the ESUs. In this case, it is important to select a representative image among the collection for the classification process.

Figure 12: ESU (6). CAN-EYE processing over an heterogeneous onion field.

4.3.2. Content of the Ground Dataset

Each ESU is described according to a standard format. The header of the database is shown in *Table 3*.
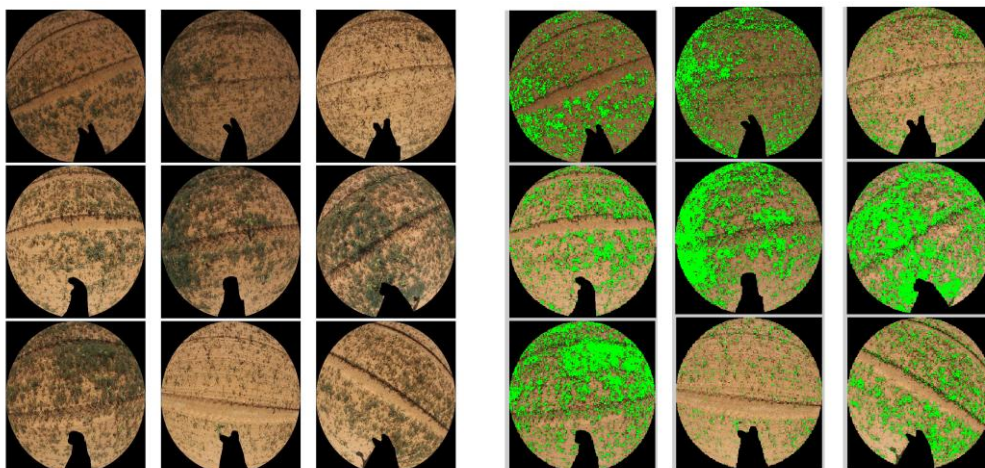
Table 3: The Header used to describe ESUs with the ground measurements.

Column	Var.Name		Comment
1	Plot #		Number of the field plot in the site
2	Plot Label		Label of the plot in the site
3	ESU #		Number of the Elementary Sampling Unit (ESU)
4	ESU Label		Label of the ESU in the campaign
5	Northing Coord.		Geographical coordinate: Latitude (⁰), WGS-84
6	Easting Coord.		Geographical coordinate: Longitude (⁰), WGS-84
7	Extent (m) of ESU (diameter)		Size of the ESU [1]
8	Land Cover		Detailed land cover
9	Start Date (dd/mm/yyyy)		Starting date of measurements
10	End Date (dd/mm/yyyy)		Ending date of measurements
11	Products*	Method	Instrument
12		Nb. Replications	Number of Replications
13		PRODUCT	Methodology
14		Uncertainty	Standard deviation

*LAIeff, LAI, FAPAR and FCOVER

Figure 13 to Figure 16 show the biophysical parameters obtained during the field experiment. Figure 13 shows the effective LAIeff, ranging between 0 (harvested winter crops) - 0.2 (corn, sunflower and other growing croplands) and 6 (Alfalfa). Maximum values were obtained for the Alfalfa field (around 6) and for the Papaver Somniferum (around 5). Rape and Wheat crops presented also high values. Similar distributions were obtained for LAI, with higher values due to the clumping factor (Figure 14). Maximum values were obtained for Alfalfa (up to 7.5) and for Papaver (up to 6). Note however that the clumping index for Alfalfa and Papaver fields was found unreliable (between 0.8 and 0.83) for these very homogeneous canopies (so clumping should be very close to 1, especially for the alfalfa crop). This should be interpreted as an uncertainty introduced in the clumping estimation by the CAN-EYE, which provides very high LAI estimates for Alfalfa and Papaver. In this particular case, we recommend to use the effective LAI as a good proxy of actual LAI. The lower values were obtained for Corn and Onion that were in very early stages of growth.

Note that for all variables, the values considered for Barley, Camelina, and Wheat (W3) were estimated with visual inspection (LAI, FAPAR and FCOVER estimated equal to zero due to its senescent stage) as the plants were in their last phenological phase, completely dry.
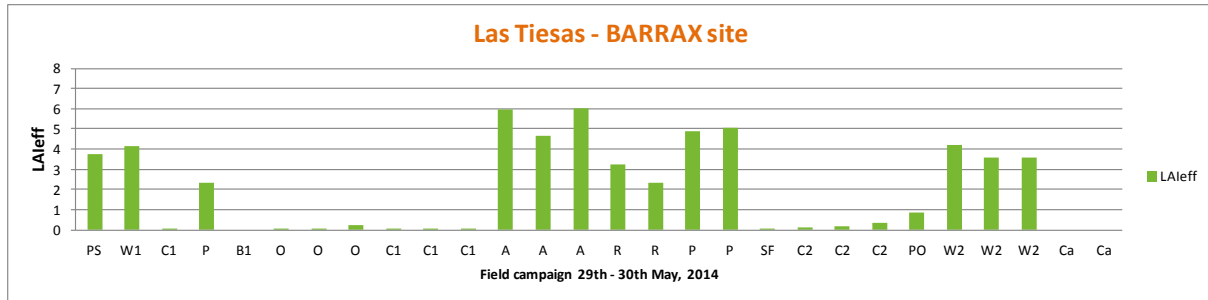
Figure 13: LAIeff measurements acquired in Las Tiesas site – Barrax, during the campaign of May 2014. A: Alfalfa, C: Corn, R: Rape, Ca: Camelina, O: Onion, PS: Papaver, P: Potato, W: Wheat and BS: Bare Soil
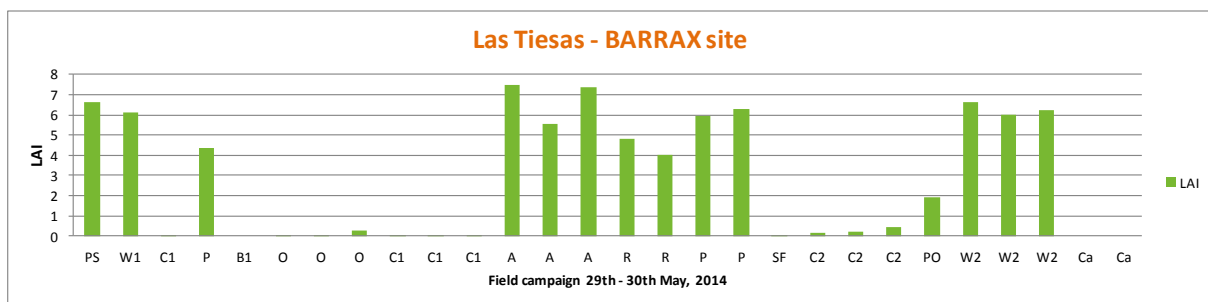
Figure 14: As in Figure 13 for LAI.

Figure 15 shows the FAPAR (instantaneous at 10 a.m. and daily integrated) values covering approximately the full dynamic range, with minimum values for corn (0.01-0.22), medium to high absorption values for potato, around 0.5 (0.43 for instantaneous and 0.55 for FAPAR daily integrated). Very similar results were found between FAPAR daily integrated and instantaneous at 10:00 am, but slightly lower for the instantaneous values at 10:00 a.m. As we obtained similar values for instantaneous FAPAR at 10 SLT and daily FAPAR integrated observations, only one map of FAPAR product has been provided (instantaneous one). Figure 16 shows the FCOVER variable, quite similar to FAPAR, full cover was obtained for Alfalfa and Papaver, and close to zero for Onion and Corn.
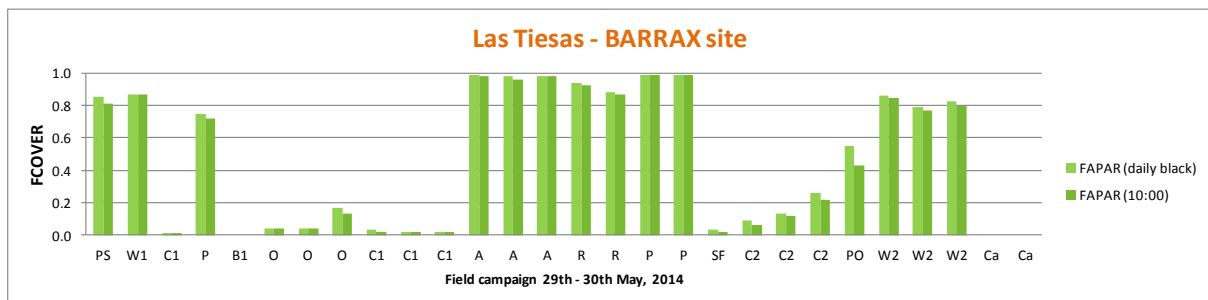
Figure 15: As in Figure 13 for FAPAR instantaneous at 10:00 am and FAPAR daily integrated measurements.

Figure 16: As in Figure 13 for FCOVER.

The distribution of the measured variables is presented in Figure 17. Note that the larger frequencies are obtained for lowest and highest values of vegetation.

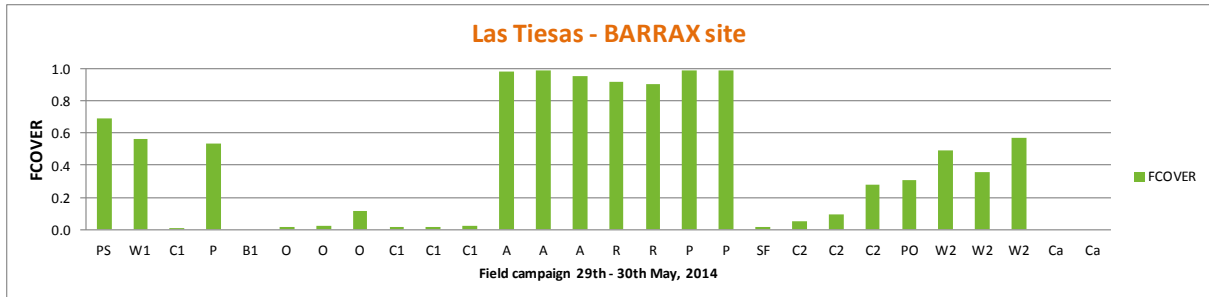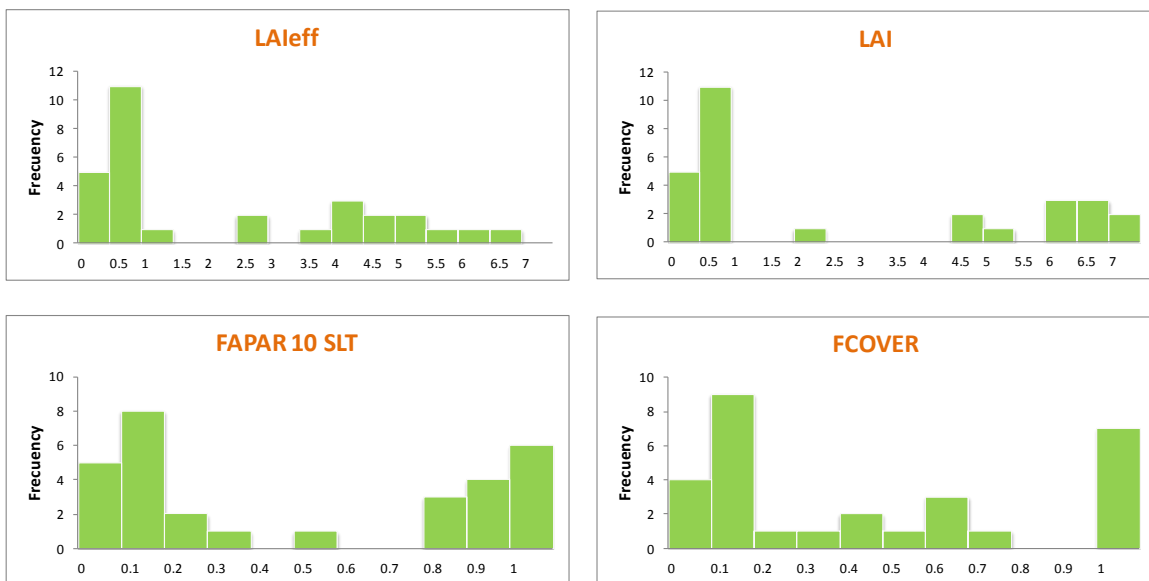**Figure 17: Distribution of the measured biophysical variables over the ESUs, Las Tiesas site – Barrax, during the campaign of 29th May, 2014**

5. EVALUATION OF THE SAMPLING

5.1. PRINCIPLES

Based on previous field activities, the data set sampling was concentrated in the most representative areas. The number of ESUs was 30 (all of them DHP), that were used for up-scaling.

5.2. EVALUATION BASED ON NDVI VALUES

The sampling strategy is evaluated using the Landsat-8 image by comparing the NDVI distribution over the site with the NDVI distribution over the ESUs (Figure 18). As the number of pixels is drastically different for the ESU and whole site (WS), it is not statistically consistent to directly compare the two NDVI histograms. Therefore, the proposed technique consists in comparing the NDVI cumulative frequency of the two distributions by a Monte-Carlo procedure which aims at comparing the actual frequency to randomly shifted sampling patterns. It consists in:

1. computing the cumulative frequency of the N pixel NDVI that correspond to the exact ESU locations; then, applying a unique random translation to the sampling design (modulo the size of the image)

2. computing the cumulative frequency of NDVI on the randomly shifted sampling design

3. repeating steps 2 and 3, 199 times with 199 different random translation vectors.

This provides a total population of N = 199 + 1(actual) cumulative frequency on which a statistical test at acceptance probability 1 - α = 95% is applied: for a given NDVI level, if the actual ESU density function is between two limits defined by the $N\alpha/2$ = 5 highest and lowest values of the 200 cumulative frequencies, the hypothesis assuming that WS and ESU NDVI distributions are equivalent is accepted, otherwise it is rejected.

Figure 18 shows that the NDVI TOC distribution of the Barrax – May, 2014 campaign is good over the whole site. Sampling is slightly biased towards high NDVI values.
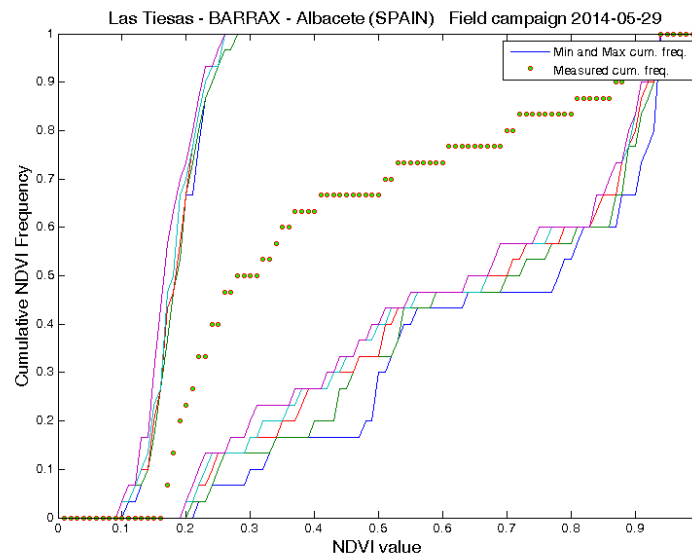
Figure 18: Comparison of NDVI TOC distribution between ESUs (green dots) and over the whole image (blue line). Field campaign Las Tiesas – Barrax (29th May 2014).

5.3. EVALUATION BASED ON CONVEX HULL: PRODUCT QUALITY FLAG.

The interpolation capabilities of the empirical transfer function used for up-scaling the ground data using decametric images is dependent of the sampling (Martinez et al., 2009). A test based on the convex hulls was also carried out to characterize the representativeness of ESUs and the reliability of the empirical transfer function using the different combinations of the selected bands (green, red, NIR and SWIR) of the Landsat-8 image. A flag image is computed over the reflectances. The result on convex-hulls can be interpreted as:

● pixels inside the 'strict convex-hull': a convex-hull is computed using all the Landsat-8 reflectances corresponding to the ESUs belonging to the class. These pixels are well represented by the ground sampling and therefore, when applying a transfer function the degree of confidence in the results will be quite high, since the transfer function will be used as an interpolator;

● pixels inside the 'large convex-hull': a convex-hull is computed using all the reflectance combinations (±5% in relative value) corresponding to the ESUs. For these pixels, the degree of confidence in the obtained results will be quite good, since the transfer function is used as an extrapolator (but not far from interpolator);

● pixels outside the two convex-hulls: this means that for these pixels, the transfer function will behave as an extrapolator which makes the results less reliable. However, having a priori information on the site may help to evaluate the extrapolation capacities of the transfer function.

Figure 19 shows the results of the Convex-Hull test (i.e., Quality Flag image) for the Las Tiesas - Barrax site over a 20x20 km^2 (left) and 5x5 km^2 (right) areas around the central coordinate site. The strict and large convex-hulls are high around the test site, 65% over the 20x20 km^2 area and 59% for 5x5 km^2 area.

Figure 19 shows an extrapolation (red areas) in some pivots like rape, alfalfa and reforestation fields.

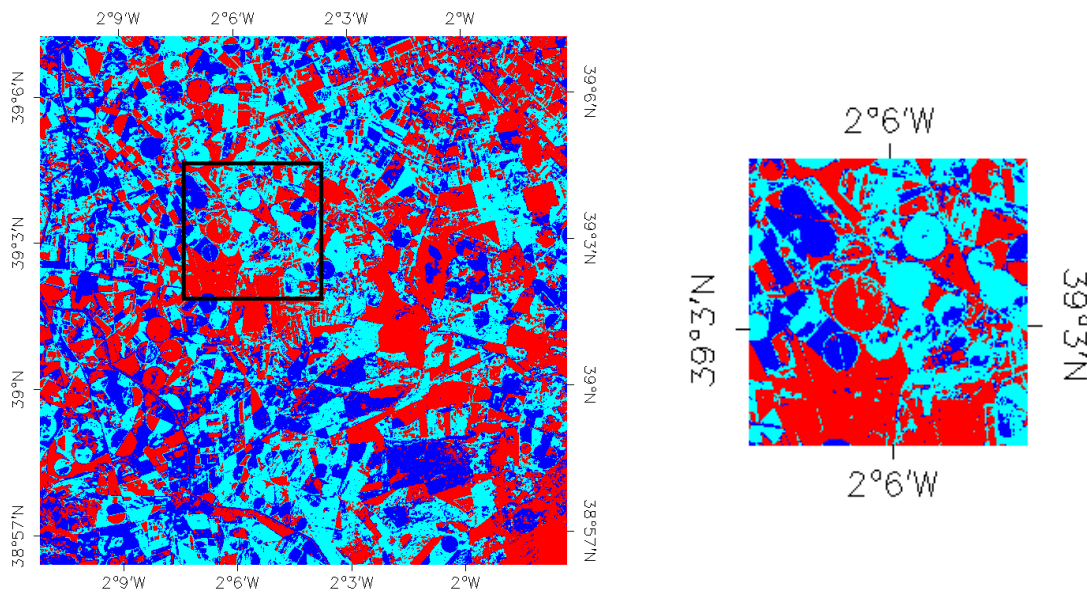**Las Tiesas site – Barrax 29th May, 2014**

Figure 19: Convex Hull test over 20x20km^2 and 5x5 km^2 areas: clear and dark blue correspond to the pixels belonging to the 'strict' and 'large' convex hulls. Red corresponds to the pixels for which the transfer function is extrapolating, Las Tiesas – Barrax (29th May 2014).

6. PRODUCTION OF GROUND-BASED MAPS

6.1. IMAGERY

The Landsat-8 images were acquired the 26th May 2014 (see *Table 4* for acquisition geometry). We selected 4 spectral bands from 500 nm to 1750 nm with a nadir ground sampling distance of 30 m. For the transfer function analysis, the input satellite data used is Top of Canopy (TOC) reflectance. The original projection is UTM 30 North, WGS-84.

Table 4: Acquisition geometry of Landsat-8 data used for retrieving high resolution maps.

Landsat-8 METADATA	
Platform / Instrument	Landsat-8 / OLI_TIRS
Path	200
Row	33
Selected Bands	B3(green) : 0.53-0.59 µm B4(red) : 0.64-0.67 µm B5(NIR) : 0.85-0.88 µm B6(SWIR1) : 1.58-1.65 µm
May 2014 campaign	
Acquisition date	2014-05-26 10:49:20
Ground control points verify	100
Geometric RMSE Verify	4.38
Illumination Azimuth angle	130.568º
Illumination Elevation angle	65.665º

6.2. THE TRANSFER FUNCTION

6.2.1. The regression method

If the number of ESUs is enough, multiple robust regression 'REG' between ESUs reflectance and the considered biophysical variable can be applied (Martínez et al., 2009): we used the 'robustfit' function from the Matlab statistics toolbox. It uses an iteratively re-weighted least squares algorithm, with the weights at each iteration computed by applying the bi-square function to the residuals from the previous iteration. This algorithm provides lower weight to ESUs that do not fit well.

The results are less sensitive to outliers in the data as compared with ordinary least squares regression. At the end of the processing, two errors are computed: weighted RMSE (using the weights attributed to each ESU) (RW) and cross-validation RMSE (leave-one-out method) (RC).

As the method has limited extrapolation capacities, a flag image (Figure 19), based on the convex hulls, is included in the final ground based map in order to inform the users on the reliability of the estimates.

6.2.2. Band combination

Figure 20 shows the results obtained for the optimal band combinations using TOC reflectances. For this campaign, we have selected the NDVI (band2 (red) and band 3 (NIR)) for the transfer function as this combination provides more consistent results for very low values. Note that Barrax area presents a large fraction of bare soils/senescent areas, and using other combination we found unreliable estimates over these problematic areas.

Las Tiesas site – Barrax 29th May, 2014

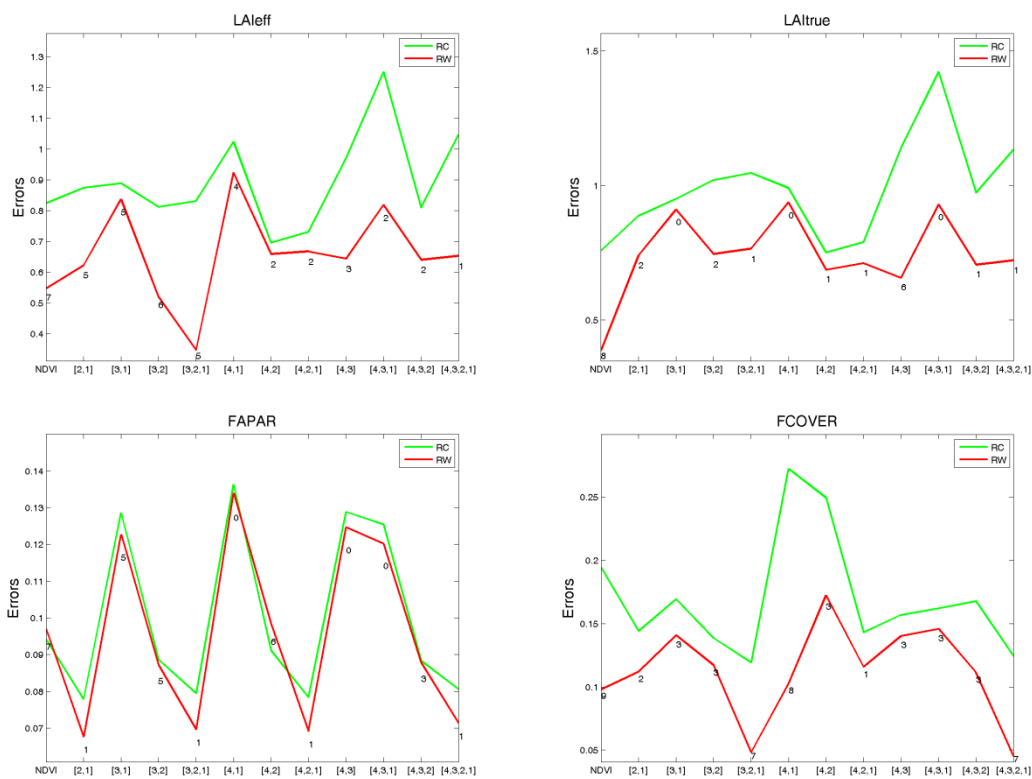**Figure 20: Test of multiple regression (TF) applied on different band combinations. Band combinations are given in abscissa (1=G, 2=RED, 3=NIR and 4=SWIR). The weighted root mean square error (RMSE) is presented in red along with the cross-validation RMSE in green. The numbers indicate the number of data used for the robust regression with a weight lower than 0.7 that could be considered as outliers.**

6.2.3. The selected Transfer Function

The applied transfer function is detailed in *Table 5*, along with its weighted and cross validated errors.

Table 5: Transfer function applied to the whole site for LAIeff, LAI, instantaneous FAPAR at 10:00 am and FCOVER. RW for weighted RMSE, and RC for cross-validation RMSE.

Variable	Band Combination	RW	RC
Field campaign of 29th – 30th May, 2014			
LAIeff	-1.022 + 5.689·(NDVI)	0.55	0.80
LAI	-1.677 + 9.552·(NDVI)	0.39	0.73
FAPAR	- 0.188 + 1.234·(NDVI)	0.10	0.09
FCOVER	- 0.214 + 1.2979·(NDVI)	0.10	0.19

Figure 21 shows scatter-plots between ground observations and their corresponding transfer function (TF) estimates for the selected bands combinations. A good correlation is observed for the LAIeff, LAI, FAPAR and FCOVER with points distributed along the 1:1 line and no bias, but showing some scattering mainly for lower values. For LAI and FAPAR there are several dots over the TF axis, which corresponds to the Corn and Sunflower ESUs in a very early stage of growing, where the empirical transfer function presents an overestimation. User should consider these two crops with caution, as the retrieved biophysical variable should be very close to zero. On the other hand, in the case of LAI, for high values, an overestimation is expected due to the overestimation of the ground LAI values as said before.

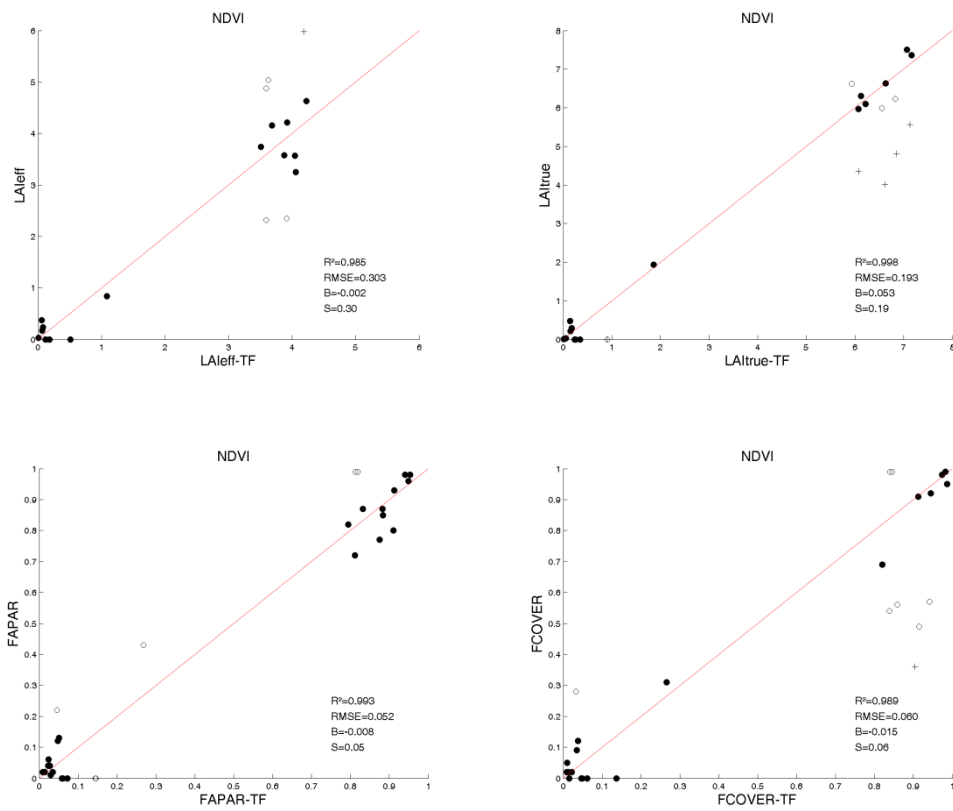**Las Tiesas site – Barrax 29th May, 2014**

Figure 21: LAIeff, LAI, FAPAR and FCOVER results for regression on reflectance using the NDVI band. Full dots: Weight>0.7. Empty dots: 0<Weight<0.7. Crosses: Weight=0.

6.3. THE HIGH RESOLUTION GROUND BASED MAPS

The high resolution maps are obtained applying the selected transfer function (Table 6) to the Landsat-8 TOC reflectance. Figure 22, Figure 23, and Figure 24 present the TF biophysical variables over a 20x20 km^2 area. The maps display a good contrast between bare/senescent areas and irrigated crops. However, the LAI ground based maps displayed many fields with very high LAI values (saturated at 7).   This result seems to be an overestimation of the actual LAI, which should be very close to the effective LAI in this site (as most of the crops in Barrax site were very homogeneous). Figure 19 shows the Quality Flag included in the final product.

Las Tiesas site – Barrax 29th May, 2014

LAIeff **LAI**

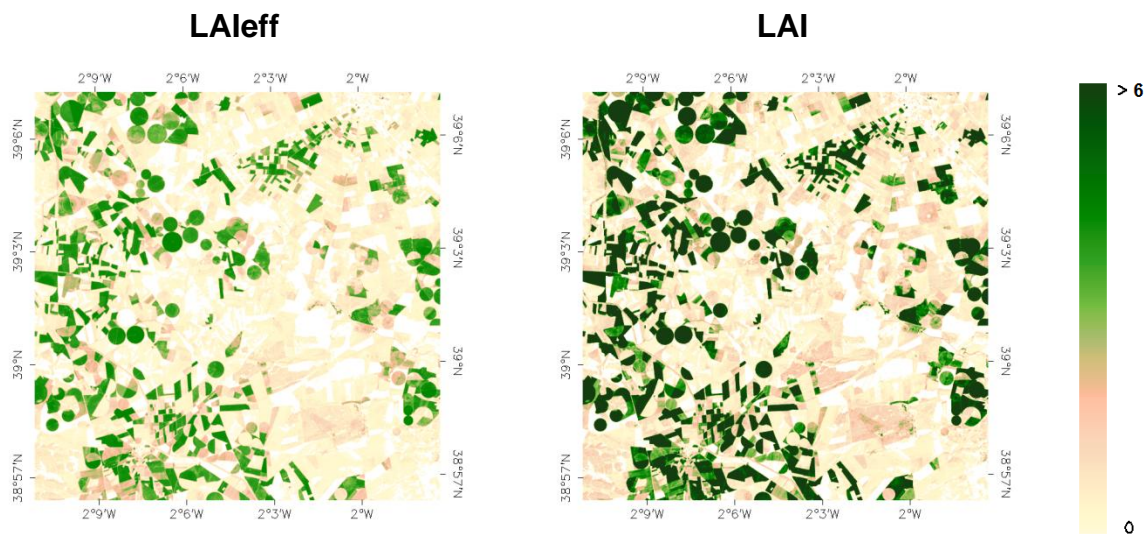**Figure 22: Ground-based LAI maps (20x20 km^2) retrieved on the Las Tiesas - Barrax site (Spain). Left: LAIeff. Right: LAI. (29th May 2014).**

Las Tiesas site – Barrax 29th May, 2014
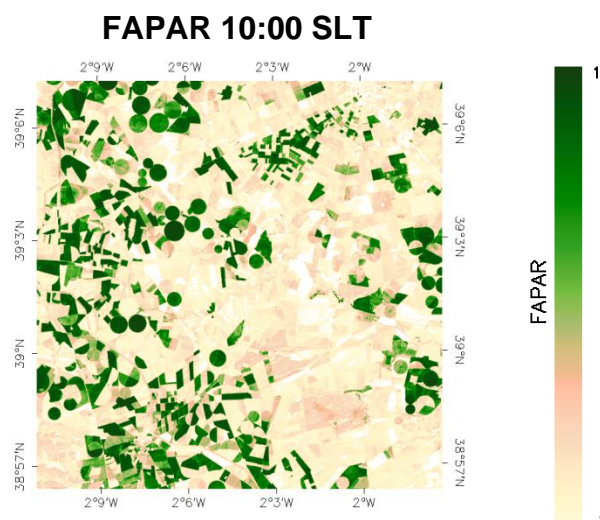
FAPAR 10:00 SLT

Figure 23: Ground-based of Instantaneous FAPAR at 10:00 a.m. maps (20x20 km^2) retrieved on the Las Tiesas - Barrax site (Spain). (29th May 2014).

Las Tiesas site – Barrax 29th May, 2014

FCOVER
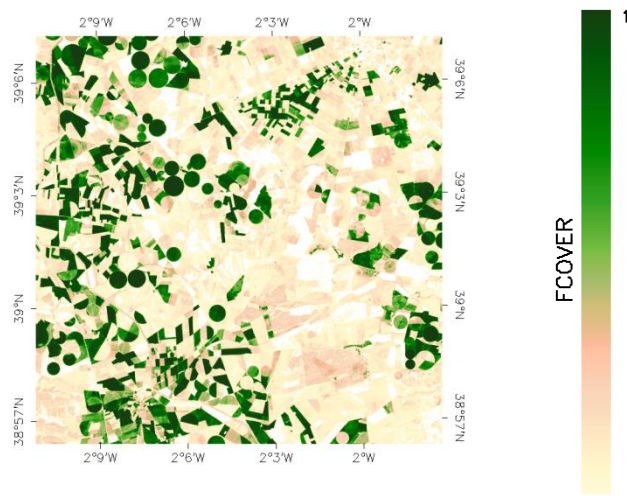
Figure 24: Ground-based FCOVER map (20x20 km^2) retrieved on the Las Tiesas site – Barrax site (Spain). (29th May 2014).

Figure 25 shows these ground-based high resolution maps over the 5x5 km^2 study area centered in Las Tiesas farm. These maps are provided for validation of satellite products at different resolutions. Mean values over 3x3 km^2 are shown in the Table 6.

Las Tiesas site – Barrax 29th May, 2014

LAIeff	LAI

FAPAR 10:00 SLT	FCOVER

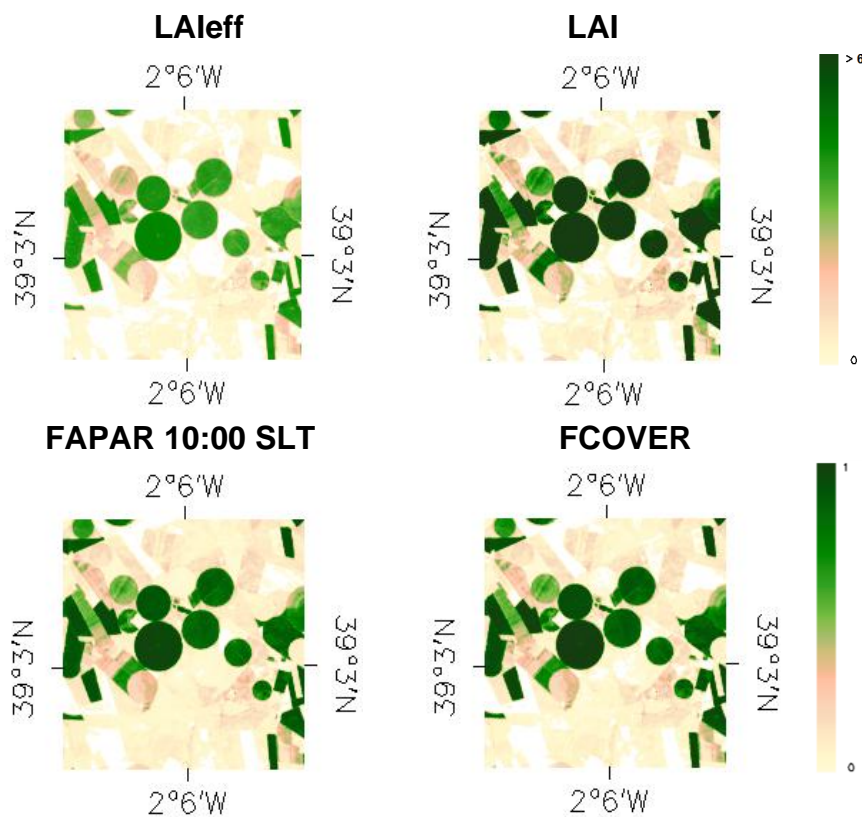**Figure 25: Ground-based maps (5x5 km^2) retrieved on the Las Tiesas - Barrax site (Spain). (20th May 2014).**

6.3.1. Mean Values

Mean values of a 3x3 km^2 area centred in the test site are provided for the validation of 1 km satellite products in agreement with the CEOS OLIVE direct dataset (*Table 6*). For the validation of coarser resolutions product (e.g. MSG products) a larger area should be considered. For this reason, empirical maps are provided at 5x5 km^2, and 20x20 km^2. The user should be cautious when considering the mean LAI value, which can overestimate the actual value. The effective LAI average value can be more accurate, and consistent also with the FCover and FAPAR values.

Table 6: Mean values and standard deviation (STD) of the HR biophysical maps for the selected 3 x 3 km2 areas at Las Tiesas site – Barrax (Spain).

3x3 km^2		Las Tiesas-Barrax	
		LATITUDE	LONGITUDE
		39.054371	-2.100677
LAIeff	MEAN	1.50	
	STD	1.61	
LAI	MEAN	2.54	
	STD	2.68	
FAPAR 10 a.m.	MEAN	0.35	
	STD	0.35	
FCOVER	MEAN	0.36	
	STD	0.36	

Table 7 describes the content of the geo-biophysical maps in the "BIO_YYYYMMDD_LANDSAT8_ Barrax_ETF_20x20" files.

Nomenclature: BIO_YYYYMMDD_SENSOR_Site_ETF_Area
where:

    BIO stands for Biophysical (LAIeff, LAI, FAPAR and FCOVER)

    SENSOR = LANDSAT8

    YYYYMMDD = Campaign date

    Site = Barrax

    ETF stands for Empirical Transfer Function

    Area = window size 20x20 and 5x5

Table 7: Content of the dataset.

Parameter	Dataset name	Range	Variable Type	Scale Factor	No Value
LAI effective	LAIeff	[0, 7]	Integer	1000	-1
LAI	LAI	[0, 7]	Integer	1000	-1
FAPAR 10:00 SLT	FAPAR	[0, 1]	Integer	10000	-1
Fraction of Vegetation Cover	FCOVER	[0, 1]	Integer	10000	-1
Quality Flag	QFlag	0,1,2 (*)	Integer	N/A	-1

$^{(*)}$ 0 means extrapolated value (low confidence), 1 strict interpolator (best confidence), 2 large interpolator (medium confidence).

7. CONCLUSIONS

The FP7 ImagineS project continues the innovation and development activities to support the operations of the Copernicus Global Land service. One of the ImagineS demonstration sites is located in Las Tiesas – Barrax, an experimental site situated within La Mancha, a plateau 700 m above sea level. The test site is located in the west of province of Albacete, Spain. It is 20 km far away from the capital town Albacete. The area is characterized by a flat morphology with large and uniform land units.

This report firstly presents the ground data collected during an intensive field campaign on 29th - 30th of May of 2014. The dataset includes 30 elementary sampling units where digital hemispherical photographs were taken and processed with the CAN-EYE software to provide LAI, LAIeff, FAPAR and FCOVER values to characterize the natural vegetation of the cultivated area. Clumping index values for the very homogeneous Alfalfa and Papaver crops were found unreliable, and so the LAI values for these canopies (very representative of the dense crops in the area) are overestimated. In addition, bare areas or non-photosynthetically active fields were identified to have a better control of these areas in the ground based maps.

Secondly, high resolution ground-based maps of the biophysical variables have been produced over the site. Ground-based maps have been derived using high resolution imagery (Landsat-8 TOC Reflectance) according with the CEOS LPV recommendations for validation of low resolution satellite sensors. Transfer functions have been derived by multiple robust regressions between ESUs reflectance and the several biophysical variables. The spectral band selected to minimize errors over bare/senescent areas was the NDVI (red, NIR bands. The RMSE values for the several transfer function estimates are 0.30 for LAIeff, 0.19 for LAI, 0.05 for instantaneous FAPAR at 10:00 h SLT and finally 0.06 for FCOVER, with very low bias. However, the values of LAI maps seem to be overestimated, as the ground estimates for very dense canopies were found very high. It is thus recommended to use effective LAI as a proxy of the actual LAI, as in this cropland area during the experiment (very homogeneous crops) the clumping index should be typically close to one.

The quality flag map based on the convex-hull analysis shows quite good quality (65 % at 20x20 km^2) with extrapolations typically over bare/senescent areas.

The biophysical variable maps are available in geographic (UTM 30 North projection WGS-84) coordinates at 30 m resolution. Mean values and standard deviation for LAIeff, LAI, FCOVER and FAPAR were computed over an area of 3x3 km^2 for validation of low and medium resolution satellite products.

8. ACKNOWLEDGEMENTS

9. REFERENCES

Baret, F and Fernandes, R. (2012). Validation Concept. VALSE2-PR-014-INRA, 42 pp.

Berguer. M. M. Rast, P. Wursteisen, E. Attema, J. Moreno, et al. (2001). The DAISEX campaigns in support of a future land-surface-processes mission. Esa bulletin, Bulletin ASE. European Space Agency, nº105: 101-111, February 2001.

Calera, A., A.M. Jochum, A. Cuesta, A. Montoro and P. López Fuster (2005). Irrigation management from space: Towards user-friendly products. Irrig. Drain. Systems, 19, 337-353.

Camacho, F., Cernicharo, J., Lacaze, R., Baret, F., and Weiss, M. (2013). GEOV1: LAI, FAPAR Essential Climate Variables and FCOVER global time series capitalizing over existing products. Part 2: Validation and intercomparison with reference products. *Remote Sensing of Environment, 137: 310-329.*

Demarez, V., Duthoit, S., Baret, F., Weiss, M. and Dedieu, G. (2008). Estimation of leaf area and clumping indexes of crops with hemispherical photographs. *Agricultural and Forest Meteorology. I48, 644-655.*

Fernandes, R., Plummer, S., Nightingale, J., et al. (2014). Global Leaf Area Index Product Validation Good Practices. CEOS Working Group on Calibration and Validation - Land Product Validation Sub-Group. *Version 2.0: Public version made available on LPV website.*

Martínez, B., García-Haro, F. J., & Camacho, F. (2009). Derivation of high-resolution leaf area index maps in support of validation activities: Application to the cropland Barrax site. *Agricultural and Forest Meteorology, 149, 130–145.*

Miller, J.B. (1967). A formula for average foliage density. Aust. J. Bot., 15:141-144

Morisette, J. T., Baret, F., Privette, J. L., Myneni, R. B., Nickeson, J. E., Garrigues, S., et al. (2006). Validation of global moderate-resolution LAI products: A framework proposed within the CEOS land product validation subgroup. *IEEE Transactions on Geoscience and Remote Sensing, 44, 1804–1817.*

Latorre, C., Camacho, F., Pérez, Beget M.E. and Di Bella, C. (2014). "Vegetation Field Data and Production of Ground-Based Maps: 25 de Mayo site. La Pampa, ARGENTINA" report. 18 -20 (Available at ImagineS website: http://fp7-imagines.eu/pages/documents.php).

Weiss, M., Baret, F., Smith, G.J., Jonckheere, I. and Coppin, P., (2004). Review of methods for in situ leaf area index (LAI) determination. Part II. Estimation of LAI, errors and sampling. *Agricultural and Forest Meteorology. 121, 37–53.*

Weiss M. and Baret F. (2010). CAN-EYE V6.1 User Manual

Welles, J.M. and Norman, J.M., 1991. Instrument for indirect measurement of canopy architecture. Agronomy J., 83(5): 818-825.